Exact, Born–Oppenheimer, and quantum-chemistry-like calculations in helium clusters doped with light molecules: The $He_2N_2(X)$ system

O. Roncero,[1] M. P. de Lara-Castells,[1] G. Delgado-Barrio,[1] P. Villarreal,[1,a)] T. Stoecklin,[2] A. Voronin,[2] and J. C. Rayez[2]
[1]*Instituto de Física Fundamental (C.S.I.C.), Serrano 123, E-28006 Madrid, Spain*
[2]*Institut des Sciences Moléculaires, UMR5255-CNRS, 351 cours de la Libération, 33405 Talence Cedex, France*

(Received 13 December 2007; accepted 28 February 2008; published online 29 April 2008)

Helium clusters doped with diatomic molecules, He_N–BC, have been recently studied by means of a quantum-chemistry-like approach. The model treats He atoms as "electrons" and dopants as "nuclei" in standard electronic structure calculations. Due to the large mass difference between He atoms and electrons, and to the replacement of Coulomb interactions by intermolecular potentials, it is worth assessing up to what extent are the approximations involved in this model, i.e., decoupling of the BC rotation from the He-atom orbital angular momenta and Born–Oppenheimer separation of the BC stretch versus the He motions, accurate enough. These issues have been previously tackled elsewhere for the $^4He_2$–$Br_2(X)$ system, which contains a heavy dopant [Roncero *et al.*, Int. J. Quantum Chem. **107**, 2756 (2007)]. Here, we consider a similar cluster but with a much lighter dopant such as $N_2(X)$. Although the model does not provide the correct energy levels for the cluster, positions and intensities of the main detectable lines of the vibrotational Raman spectrum at low temperature are accurately reproduced. © *2008 American Institute of Physics*. [DOI: 10.1063/1.2900560]

I. INTRODUCTION

Since the pioneering experiments on the infrared (IR) spectra of the SF_6 (Refs. 1 and 2) molecule embedded in helium droplets, further advances in the synthesis and characterization of solvated molecular species[3,4] have stimulated the spectroscopic study of different molecules in ultracold environments. Thus, the rotationally resolved IR spectra of different molecules in helium nanodroplets[5–7] and high-resolution IR measurements on CO in small helium clusters[8,9] have been recently reported. Among all this experimental information, the IR spectra of oxygen carbon sulfide (OCS) (Refs. 10 and 11) constitute a highly challenging example, since interesting features related to the intrinsic quantum nature of the solvent seem to play a crucial role. On the one hand, when OCS is solvated in the fermionic ^{3}He nanodroplet, the spectrum exhibits an unstructured broad shape, as one might expect in the case of heavy molecules immersed in liquids. Surprisingly, on the other hand, the spectrum of OCS in the bosonic ^{4}He nanodroplet displays well-defined *P* and *R* branches and resembles the gas-phase spectrum of the OCS molecule. In fact, the molecule seems to be almost freely rotating in the bosonic solvent, therefore, reflecting the superfluidity, at a microscopic scale, of the ^{4}He nanodroplet.[10,11]

These experimental achievements have been accompanied by detailed theoretical investigations for the ground-state structure and energetics of helium clusters. In this regard, valuable information about relevant properties of such aggregates is provided by zero temperature diffusion Monte Carlo and finite temperature Feynman path-integral Monte Carlo calculations (see Ref. 12 for a review).

An alternative quantum-chemistry (QC)-like approach, which is originally applied to the lowest triplet state of the SF_6–$(^3He)_2$ cluster,[13] has been developed to study diatomic molecules embedded in helium clusters. In particular, the energy levels and structure properties of He_N–BC(X) complexes,[14–19] where *N* is a large number ($N \simeq 30, 60$) of either boson or fermion helium atoms and BC stands for a heavy dihalogen molecule as Br_2 or ICl, have been recently investigated. One of the main advantages of this method consists in providing bound state wave functions for these clusters. Simulations of the spectra can therefore be obtained and compared with the experimental results. The main approximations involved in these kinds of calculations (the decoupling of the He-atom orbital angular momenta from the diatomic rotation, and the adiabaticity with respect to the diatomic vibration) have been tested for the ^4He_N–Br_2, $N=2$ cluster.[20] This is an amenable system to perform variational (exact) calculations[21–27] for which extensions up to $N=5$ have been recently carried out.[28] In this paper, we consider a similar system but containing a lighter dopant, such as the $^4He_2$–N_2 cluster. This is a more critical scenario where the use of the above mentioned approximations deserves a careful analysis.

This paper is organized as follows. In Sec. II, the most relevant details of the theoretical treatment employed, such as the Hamiltonian, the symmetry-adapted basis functions, and the different approaches, are described. Section II also includes the theoretical simulation of vibrotational Raman

a)Author to whom correspondence should be addressed. Electronic mail: p.villarreal@imaff.cfmac.csic.es.

spectra. In Sec. III, we characterize the potential energy surface (PES) employed and provide the details of the numerical calculations. The results obtained are shown in Sec. IV. Finally, a summary and an outlook of the present work are outlined in Sec. V.

II. THEORETICAL MODEL

A. Hamiltonian and wave functions

The Hamiltonian describing the He_2–BC system can be written in satellite coordinates $\{(\mathbf{r},\mathbf{R}_k)\}$ as[21]

$$H = H^d + \sum_{k=1}^{2} H_k^t(\mathbf{R}_k,r) + \tilde{V}_{12}, \tag{1}$$

where $\mathbf{r}$ is the vector joining the B and C atoms and $\mathbf{R}_k$ are the vectors from the BC molecule center of mass to the different He atoms. H^d is the Hamiltonian of the BC molecule,

$$H^d = -\frac{\hbar^2}{2m}\frac{\partial^2}{\partial r^2} + U(r) + \frac{\mathbf{j}^2}{2mr^2}, \tag{2}$$

where m is the reduced mass, $\mathbf{j}$ is the angular momentum associated with $\mathbf{r}$, and U represents the intramolecular diatomic potential. H_k^t, $(k=1,2)$, are triatomic Hamiltonians of the form

$$H_k^t(\mathbf{R}_k,r) = -\frac{\hbar^2}{2\mu}\frac{\partial^2}{\partial R_k^2} + \frac{\mathbf{l}_k^2}{2\mu R_k^2} + W(R_k,r,\theta_k), \tag{3}$$

where μ is the reduced mass of the He–BC system, $\mathbf{l}_k$ is the angular momentum associated with $\mathbf{R}_k$, and W represents the atom-diatom intermolecular potential that depends on the pair of (R_k,r) distances and on the angle θ_k between the $\mathbf{R}_k$ and $\mathbf{r}$ vectors. Finally, in Eq. (1), $\tilde{V}_{12}$ describes He–He interactions

$$\tilde{V}_{12} = V_{12}(|\mathbf{R}_k - \mathbf{R}_l|) - \frac{\hbar^2}{m_B + m_C}\nabla_1 \cdot \nabla_2, \tag{4}$$

which includes the He–He potential V_{12} and a kinetic energy coupling term arising from the use of non-Jacobi coordinates.

We choose a body-fixed (BF) frame with the Z^{BF} axis parallel to $\mathbf{r}$, and introduce the quantum numbers associated with the helium orbital angular momentum $\mathbf{l}_k$, ℓ_k, and the He–BC vibration n_k, collectively denoted by $\{q_k\}=\{\ell_k n_k\}$ $(k=1,2)$. The basis functions are expressed as[21]

$$\Psi^{JM\Omega}_{v q_1 q_2 L}(\mathbf{r},\mathbf{R}_1,\mathbf{R}_2) = \chi_v(r)\Phi^{JM}_{q_1 q_2 L\Omega}(\hat{\mathbf{r}},\mathbf{R}_1,\mathbf{R}_2), \tag{5}$$

where L is the quantum number associated with the total orbital angular momentum $\mathbf{L}=\mathbf{l}_1+\mathbf{l}_2$, χ_v is a vibrational state of the (nonrotating) diatomic molecule

$$\left[-\frac{\hbar^2}{2m}\frac{\partial^2}{\partial r^2} + U(r) - \epsilon_v\right]\chi_v(r) = 0, \tag{6}$$

and

$$\Phi^{JM}_{q_1 q_2 L\Omega}(\hat{\mathbf{r}},\mathbf{R}_1,\mathbf{R}_2) = f_{n_1}(R_1) f_{n_2}(R_2)\mathcal{W}^{JM}_{\ell_1\ell_2 L\Omega}(\hat{\mathbf{r}},\hat{\mathbf{R}}_1,\hat{\mathbf{R}}_2). \tag{7}$$

Here, f_{n_i} are the radial functions associated with the He–BC stretching motions which will be specified later on. In Eq. (7), the angular functions $\mathcal{W}^{JM}_{\ell_1\ell_2 L\Omega}$ depend on the diatomic orientation $\hat{\mathbf{r}}\equiv(\theta_r,\phi_r)$ with respect to a space-fixed (SF) reference system, and on the orientations $\hat{\mathbf{R}}_k\equiv(\theta_k,\phi_k)$ in the BF frame. They are expressed as

$$\mathcal{W}^{JM}_{\ell_1\ell_2 L\Omega}(\hat{\mathbf{r}},\hat{\mathbf{R}}_1,\hat{\mathbf{R}}_2) = \sqrt{\frac{2J+1}{4\pi}}\mathcal{D}^{J*}_{M\Omega}(\phi_r,\theta_r,0)\mathcal{Y}^{L\Omega}_{\ell_1\ell_2}(\hat{\mathbf{R}}_1,\hat{\mathbf{R}}_2), \tag{8}$$

where $\mathcal{D}^J_{M\Omega}$ are Wigner rotation matrices labeled by J, the quantum number associated with the total angular momentum $\mathbf{J}=\mathbf{j}+\mathbf{L}$, and by M and Ω, the quantum numbers associated with the projections of $\mathbf{J}$ on Z^{SF} and Z^{BF}, respectively. In turn, $\mathcal{Y}^{L\Omega}_{\ell_1\ell_2}$ are angular functions in the coupled representation,

$$\mathcal{Y}^{L\Omega}_{\ell_1\ell_2}(\hat{\mathbf{R}}_1,\hat{\mathbf{R}}_2) = (-1)^{L+\Omega}\sqrt{2L+1} \times\sum_{\omega}\begin{pmatrix}\ell_1 & \ell_2 & L\\ -\omega & \omega-\Omega & \Omega\end{pmatrix} \times Y_{\ell_1\omega}(\theta_1,\phi_1)Y_{\ell_2\Omega-\omega}(\theta_2,\phi_2), \tag{9}$$

where (:::) are $3-j$ symbols and $Y_{\ell_i\omega}(\theta_i,\phi_i)$ are spherical harmonics.

The relevant symmetry operators of the system are those corresponding to the total inversion $\mathcal{E}^*$, the permutation of the He atoms $\mathcal{P}_{12}$, and, if BC is homonuclear, the exchange of diatomic nuclei $\mathcal{P}_{BC}$. The action of these operators over the basis functions written in Eq. (5) is[21]

$$\mathcal{E}^*[\Psi^{JM\Omega}_{v q_1 q_2 L}] = (-1)^{J+\ell_1+\ell_2+L}\Psi^{JM-\Omega}_{v q_1 q_2 L}, \tag{10}$$

$$\mathcal{P}_{12}[\Psi^{JM\Omega}_{v q_1 q_2 L}] = (-1)^{\ell_1+\ell_2+L}\Psi^{JM\Omega}_{v q_2 q_1 L}, \tag{11}$$

and

$$\mathcal{P}_{BC}[\Psi^{JM\Omega}_{v q_1 q_2 L}] = (-1)^{J+L}\Psi^{JM-\Omega}_{v q_1 q_2 L}. \tag{12}$$

It is then possible to define a symmetry-adapted basis set as

$$\Psi^{JM\Omega\varepsilon\kappa\eta}_{v q_1 q_2 L} = \chi_v\Phi^{JM\varepsilon\kappa\eta}_{q_1 q_2 L\Omega}, \tag{13}$$

where

$$\Phi^{JM\varepsilon\kappa\eta}_{q_1 q_2 L\Omega} = \mathcal{N}\{[\Phi^{JM}_{q_1 q_2 L\Omega} + \varepsilon\kappa\eta(-1)^L\Phi^{JM}_{q_2 q_1 L\Omega}] + (-1)^J[\eta(-1)^L\Phi^{JM}_{q_1 q_2 L-\Omega} + \varepsilon\kappa\Phi^{JM}_{q_2 q_1 L-\Omega}]\}, \tag{14}$$

$\Omega \geqslant 0$, and $\mathcal{N}=(1/2)\ [(1+\delta_{\Omega 0})(1+\delta_{n_1 n_2}\delta_{\ell_1\ell_2})]^{-1/2}$ is a normalization factor. The $\Psi^{JM\Omega\varepsilon\kappa\eta}_{v q_1 q_2 L}$ are eigenfunctions of $\mathcal{E}^*$, $\mathcal{P}_{12}$, and $\mathcal{P}_{BC}$, with eigenvalues ε, κ, and $\eta=\varepsilon(-1)^{\ell_1+\ell_2}$, respectively.

B. Diabatic, adiabatic, and quantum-chemistry-like treatments

In an exact treatment, for the given values of $\{J,\varepsilon,\kappa,\eta\}$, the wave function is expanded in terms of the basis functions of Eq. (13) where the corresponding sum runs over v,q_1,q_2,L,Ω quantum numbers up to convergence. However, due to the mismatch existing between the low-frequency He–BC stretching/bending motions and the high-frequency BC vibrations, one may consider just a single diatomic vibration in the aforementioned expansion. The total wave function is then approximated by means of the following diabatic (D) wave function as

$$\Psi^{\mathrm{D}} \simeq \chi_v(r)\Phi^{\mathrm{D}}_{JM}(\mathbf{R}_1,\mathbf{R}_2,\hat{\mathbf{r}}) = \chi_v(r)\sum_{q_1q_2L\Omega} c_{q_1q_2L\Omega}\Phi^{JM}_{q_1q_2L\Omega}(\hat{\mathbf{r}},\mathbf{R}_1,\mathbf{R}_2), \tag{15}$$

where the $c_{q_1q_2L\Omega}$ coefficients are obtained by solving the Schrödinger equation associated with the effective Hamiltonian

$$H^{(v)} = -\frac{\hbar^2}{2\mu}\frac{\partial^2}{\partial R_1^2} + \frac{\mathbf{l}_1^2}{2\mu R_1^2} + W_v(R_1,\theta_1) - \frac{\hbar^2}{2\mu}\frac{\partial^2}{\partial R_2^2} + \frac{\mathbf{l}_2^2}{2\mu R_2^2} + W_v(R_2,\theta_2) + B_v\mathbf{j}^2 + \tilde{V}_{12}, \tag{16}$$

whose eigenvalues are denoted by E^D_{vJ}. In Eq. (16), the vibrational diatomic function χ_v is used to average out the triatomic He–BC potentials, $W_v(R_k,\theta_k)=\langle\chi_v|W(R_k,r,\theta_k)|\chi_v\rangle$ and to obtain an effective diatomic rotational constant $B_v=\langle\chi_v|r^{-2}|\chi_v\rangle$. This constitutes the D vibrational approach, first proposed for triatomic systems[29] and also applied to tetratomic van der Waals complexes.[21,23] This approach assumes that the diatomic vibration remains unchanged inside the cluster and is expected to be accurate for the lower diatomic vibrational states. Within this framework, the total energy of the system is $E^D_{vJ}+\epsilon_v$.

In the adiabatic (AD) or Born–Oppenheimer approximation, one retains the rotational term of the diatomic Hamiltonian H^d given in Eq. (2), and then solves the Schrödinger equation

$$\left[\sum_{k=1}^{2} H^t_k(\mathbf{R}_k;r) + \frac{\mathbf{j}^2}{2mr^2} + \tilde{V}_{12} - E^{\mathrm{AD}}_J(r)\right]\Phi^{\mathrm{AD}}_{JM}(\mathbf{R}_1,\mathbf{R}_2,\hat{\mathbf{r}};r) = 0 \tag{17}$$

for different fixed values of the diatomic bond length r. In this equation,

$$\Phi^{\mathrm{AD}}_{JM} = \sum_{q_1q_2L\Omega} c_{q_1q_2L\Omega}(r)\Phi^{JM}_{q_1q_2L\Omega}(\hat{\mathbf{r}},\mathbf{R}_1,\mathbf{R}_2),$$

and each r-dependent eigenenergy $E^{\mathrm{AD}}_J(r)$ constitutes an additional potential energy term for the diatomic molecule. The wave function is expressed as a simple product

$$\Psi^{\mathrm{AD}} \simeq \chi^{\mathrm{AD}}_{Jv}(r)\Phi^{\mathrm{AD}}_{JM}(\mathbf{R}_1,\mathbf{R}_2,\hat{\mathbf{r}};r), \tag{18}$$

where the χ^{AD}_{Jv} functions describe the vibrational states of a distorted diatomic molecule. They are solutions of the Schrödinger equation

$$\left[-\frac{\hbar^2}{2m}\frac{\partial^2}{\partial r^2} + U(r) + E^{\mathrm{AD}}_J(r) - \varepsilon^{\mathrm{AD}}_{Jv}\right]\chi^{\mathrm{AD}}_{Jv}(r) = 0, \tag{19}$$

where v is the vibrational quantum number. Note that now the total energy of the system becomes $\varepsilon^{\mathrm{AD}}_{Jv}$.

The QC treatment, in turn, starts from the AD approach, but completely neglects the diatomic Hamiltonian, i.e., BC plays the role of fixed "nuclei." Thus, for the given r values, one solves

$$\left[\sum_{k=1}^{2} H^t_k(\mathbf{R}_k;r) + \tilde{V}_{12} - E^{\mathrm{QC}}(r)\right]\psi^{\mathrm{QC}}(\mathbf{R}_1,\mathbf{R}_2;r) = 0, \tag{20}$$

where

$$\psi^{\mathrm{QC}} = \sum_{q_1q_2L\Omega} c_{q_1q_2L\Omega}(r) f_{n_1}(R_1) f_{n_2}(R_2)\mathcal{Y}^{L\Omega}_{\ell_1\ell_2}(\hat{\mathbf{R}}_1,\hat{\mathbf{R}}_2).$$

Again, the wave function is a simple product

$$\Psi^{\mathrm{QC}} \simeq \chi^{\mathrm{QC}}_{J\Omega v}(r)\sqrt{\frac{2J+1}{4\pi}}\mathcal{D}^{J*}_{M\Omega}(\varphi_r,\theta_r,0)\psi^{\mathrm{QC}}(\mathbf{R}_1,\mathbf{R}_2;r), \tag{21}$$

where the $\chi^{\mathrm{QC}}_{J\Omega_v}(r)$ functions are obtained by solving

$$\left[-\frac{\hbar^2}{2m}\frac{\partial^2}{\partial r^2} + U(r) + E^{\mathrm{QC}}(r) + \frac{\langle\mathbf{j}^2\rangle}{2mr^2} - \varepsilon^{\mathrm{QC}}_{J\Omega v}\right]\chi^{\mathrm{QC}}_{J\Omega v}(r) = 0. \tag{22}$$

Thus, one considers a distortion of the diatomic potential which includes, in addition to $E^{\mathrm{QC}}(r)$ an average of the diatomic rotation[14,15,17]

$$\langle\mathbf{j}^2\rangle \approx \langle\mathbf{L}^2\rangle + \hbar^2[J(J+1) - 2\Omega^2], \tag{23}$$

where Coriolis couplings are neglected. The $\mathbf{L}^2$ average is computed by using the distribution of L values[21] in the ψ^{QC} state. In Eq. (23), Ω is a good quantum number determined after solving Eq. (20). In this approach, the total energy of the system is then $\varepsilon^{\mathrm{QC}}_{J\Omega_v}$.

The computational costs of the D and AD approaches are roughly comparable (the latter linearly scales with the number of points accounted for in the adiabatic variable). On the other hand, neglecting Coriolis couplings in the QC approach, which is independent of the total angular momentum J, significantly reduces the size of the matrices to be diagonalized. This becomes crucial for $J>0$ states of larger clusters, where the number of basis functions (in D or AD approaches) dramatically increases with the number of helium atoms.

C. Vibrotational Raman spectrum

We consider a process of the type

$$\mathrm{He_2} - \mathrm{N_2}(i) + \hbar\omega_0 \rightarrow \mathrm{He_2} - \mathrm{N_2}(f) + \hbar\omega_{fi}, \tag{24}$$

where an incident photon of energy $\hbar\omega_0$ induces an electric

dipole on the polarizable system. The latter, which was initially in a state $|i\rangle$, eventually radiates a photon at an energy $\hbar\omega_{fi}$ and emerges in a final state $|f\rangle$. Cross-section profiles for this process in terms of the polarizability of the dopant, which is assumed to be unaffected by complexation, have already been formulated in the frame of the QC approach.[14,15] Following a similar treatment, we use here "exact" variational wave functions expanded in the basis set of Eq. (13). We consider a scenario in which the incident light is linearly polarized, so its electric vector defines the SF Z direction. It propagates along the Y axis while the scattered light is detected along the X axis. In these conditions, the SF components of the induced dipole μ_k can be expressed as a function of the BF components of the polarizability α_m as[14,15]

$$\mu_k \sim \sum_{m=-1}^{1} (-1)^m \alpha_m \sum_{n=0}^{2} (2n+1) \begin{pmatrix} 1 & 1 & n \\ -m & m & 0 \end{pmatrix} \begin{pmatrix} 1 & 1 & n \\ -k & 0 & k \end{pmatrix} \times \mathcal{D}^n_{0-k}(\varphi_r, \theta_r, 0). \tag{25}$$

In the above expression, the index n runs over only even values for $k=0$. Using the integral over three Wigner matrices where the azimuthal variable is absent

$$\int d\tau \mathcal{D}^{J'}_{M'\Omega'} \mathcal{D}^n_{0-k} \mathcal{D}^{J*}_{M\Omega} = 4\pi \delta_{M'M} (-1)^M \begin{pmatrix} J & n & J' \\ -M & 0 & M \end{pmatrix} \times \begin{pmatrix} J & n & J' \\ -\Omega & -k & \Omega' \end{pmatrix},$$

and considering the r-independent parts of the symmetry functions of Eq. (14), one finds,

$$\langle \Phi' | \mathcal{D}^n_{0-k} | \Phi \rangle = \delta_{k0} \delta_{M'M} \delta_{\Omega'\Omega} \delta_{L'L} \sqrt{(2J'+1)(2J+1)} (-1)^M \begin{pmatrix} J & n & J' \\ -M & 0 & M \end{pmatrix} \begin{pmatrix} J & n & J' \\ -\Omega & 0 & \Omega \end{pmatrix} \{(1+\kappa\varepsilon\kappa'\varepsilon')(1+\eta\eta')[\delta_{q_1 q_1'} \delta_{q_2 q_2'} + (-1)^{J+L} \delta_{\Omega 0} \delta_{q_1 q_2'} \delta_{q_2 q_1'}] + (\kappa\varepsilon + \kappa'\varepsilon')(\eta + \eta')[(-1)^L \delta_{q_1 q_1'} \delta_{q_2 q_2'} + (-1)^J \delta_{\Omega_i 0} \delta_{q_1 q_2'} \delta_{q_2 q_1'}]\}, \tag{26}$$

which implies, besides the conservation of the M, Ω, and L quantum numbers, that only the $k=0$ component of the induced dipole moment will be nonzero. Also note that it will be zero unless $\eta=\eta'$ and $\kappa\varepsilon=\kappa'\varepsilon'$. The products of $\delta_{qq'}$ in Eq. (26) imply that $\ell_1+\ell_2=\ell_1'+\ell_2'$. Hence, taking into account that $\eta=(-1)^{\ell_1+\ell_2}\varepsilon$, it follows $\varepsilon=\varepsilon'$ and, moreover, $\kappa=\kappa'$.

The matrix elements of the unique existing induced dipole moment component between basis functions of type (13) take the form

$$\langle \Psi' | \mu_0 | \Psi \rangle = 4(-1)^M \delta_{M'M} \delta_{\Omega'\Omega} \delta_{L'L} \delta_{\varepsilon'\varepsilon} \delta_{\kappa'\kappa} \delta_{\eta'\eta} \sqrt{(2J'+1)(2J+1)} \{[1+(-1)^{J+L}\delta_{\Omega 0}]\delta_{q_1' q_1} \delta_{q_2' q_2} + [(-1)^L + (-1)^J \delta_{\Omega 0}] \delta_{q_1' q_2} \delta_{q_2' q_1}\} \left\{ \langle \chi_{v'} | \alpha | \chi_v \rangle \begin{pmatrix} J & 0 & J' \\ -M & 0 & M \end{pmatrix} \begin{pmatrix} J & 0 & J' \\ -\Omega & 0 & \Omega \end{pmatrix} + \frac{2}{3} \langle \chi_{v'} | \beta | \chi_v \rangle \begin{pmatrix} J & 2 & J' \\ -M & 0 & M \end{pmatrix} \begin{pmatrix} J & 2 & J' \\ -\Omega & 0 & \Omega \end{pmatrix} \right\}, \tag{27}$$

where $\alpha=(\alpha_0+2\alpha_1)/3$ and $\beta^2=(\alpha_0-\alpha_1)^2$ are the spherical and the anisotropic parts of the polarizability,[30] respectively. By considering the expansion of the initial and final total wave functions in terms of symmetry-adapted functions, one finally obtains

$$\mu_0^{f,i} = \sum_{v' q_1' q_2'} \sum_{v q_1 q_2} \sum_{L\Omega} A^{J_f M_i \varepsilon\kappa\eta}_{v' q_1' q_2' L\Omega} A^{J_i M_i \varepsilon\kappa\eta}_{v q_1 q_2 L\Omega} \langle \Psi_f | \mu_0 | \Psi_i \rangle, \tag{28}$$

where the A's are the coefficients of the expansion. Note the similarity of the precedent expressions, Eqs. (27) and (28), and those already obtained within the QC approach (see Refs. 14 and 15). It is found that the scattered light emerges polarized along Z^{SF}, i.e., a parallel signal should be detected. Moreover, for $\Omega=0$, one obtains diatomiclike selection rules $\Delta J=0,\pm 2$, allowing only the presence of O, Q, and S branches in the spectrum. For a fixed energy $\hbar\omega_0$ of the incident photon we introduce a Boltzmann distribution over cluster states at a given temperature T and average over initial rotational states. Hence, a line of intensity

$$I_{fi}(T) \propto \frac{e^{-(\varepsilon_i/kT)}}{\Sigma_i e^{-(\epsilon_i/kT)}} \frac{1}{2J_i+1} \sum_{M_i} |\mu_0^{f,i}|^2 \tag{29}$$

would appear at an energy $\hbar\omega_{fi}=\hbar\omega_0-(\epsilon_f-\epsilon_i)$ of the scattered photon.

III. PES AND NUMERICAL DETAILS

A. Potential energy surface

For He_2-Br_2 and He_2-ICl complexes, it has been shown that model PESs constructed as a sum of *ab initio* He–BC triatomic potentials[31–33] plus the He–He pair interaction accurately reproduces the *ab initio* points corresponding to the most relevant geometries of the entire systems.[27,34]

Here, we assume the same model to represent the PES and describe the $He-N_2$ intermolecular potential by using a recently improved version[35] of the three-dimensional *ab initio* surface reported by some of us.[36] In Ref. 35, the surface was systematically compared to all the other existing models for the well documented $He-N_2$ interaction. In particular, its

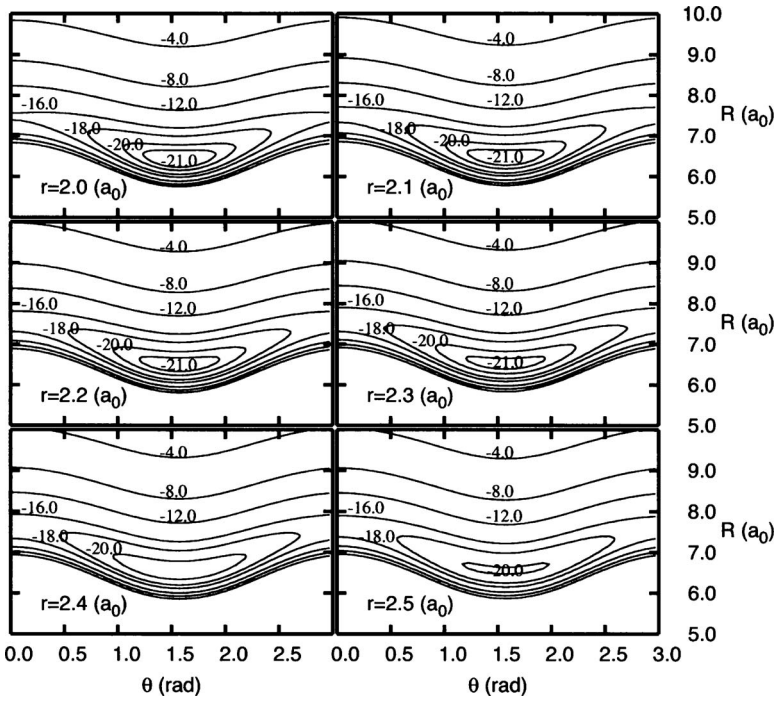

FIG. 1. Contour plots of the He–N_2 potential energy surface in Jacobi coordinates for different N–N bond distances.

ability to predict all the experimental scattering cross sections and various bulk gas properties available was carefully tested and proved to be satisfactory. Since all the details of the calculations are described in Ref. 35, here, we briefly point out the main features of the PES. A grid of 790 *ab initio* points was calculated by using the coupled cluster method with perturbative triple excitation [BCCD(T)] and Brueckner orbitals in the supermolecular approach. The global analytical form of the He–N_2(X) PES was obtained using the reproducing kernel Hilbert space method of Ho and Rabitz[37] as described in detail in Ref. 36. Contour plots of the resulting potential for the He atom moving around the N_2(X) molecule are shown in Fig. 1 for different values of the N–N distance. The most stable structure is found to be T-shaped ($\theta=90°$), the corresponding well depth being $D_e=21.73$ cm^{-1} for $r=2.0743a_0$ and $R=6.44a_0$. For linear configurations, the energy of the two equivalent saddle points, occurring at $R=7.5a_0$, is found to be -16.43 cm^{-1}. Therefore, the angular anisotropy of the surface appears to be rather small. However, an interesting feature of this PES (see Fig. 1) is the variation of its acuteness in the vicinity of the global minimum. The surface is slightly sharper at $r=2.0743a_0$ than at longer distances up to a value of $r\approx 2.3a_0$. This has an effect on the binding energies of the tri- and tetra-atomic complexes as either r or the N_2 vibrational excitation vary, as will be noted below.

The same analytical representation of the N_2(X) diatomic potential U described in Ref. 36, which was also used in our recent study,[35] is employed in the present work. It is based on the extended Hartree–Fock approximate correlation energy model.[38] In turn, the He–He interaction is described by a Morse potential function with the following parameters:[39] well depth $D_e=7.61$ cm^{-1}, characteristic inverse length $\alpha=2.126$ Å^{-1}, and equilibrium distance $R_{\rm eq}=2.963$ Å. Although this simple choice is good enough for the purposes of the present work, it would be advisable to use the more accurate He–He potentials[40] to perform a proper comparison with possible experiments.

B. Numerical details

In the calculations presented here, the following masses (amu) were used: $m_{\rm N}=14.006\,74$ and $m_{^4{\rm He}}=4.002\,60$.

The radial $f_n(R)$ functions appearing in Eq. (7) were obtained as follows. Fixing the N_2 bond length at its equilibrium value, $r_{\rm eq}=2.0743a_0$, we look for the ground level of the triatomic He–N_2 subsystem at different fixed orientations θ_n by solving the Schrödinger equation

$$\left[-\frac{\hbar^2}{2\mu}\frac{\partial^2}{\partial R^2}+W(R,\theta_n,r_{\rm eq})-E_n\right]g_n(R,\theta_n)=0. \tag{30}$$

The $g_n(R,\theta_n)$ functions are further orthogonalized through a Schmidt procedure, which leads to an orthonormal set of $f_n(R)$ functions. A grid of 4096 points in the R range of 1.5–18.5 Å was employed to numerically solve Eq. (30) using a Numerov procedure. For a proper description of the neighborhood around the equilibrium angular region, the θ_n values chosen are $\theta_n=\pi/2-(n-1)\pi/48$, $n=1$, $n_{\rm max}$. Energy convergence to within 10^{-3} cm^{-1} was achieved by using $\ell_{\rm max}=12$, $L_{\rm max}=9$, and $n_{\rm max}=4$.

For all the operators involved, the corresponding matrix elements in the present coupled representation can be found in Ref. 21. The triatomic interactions W in Eq. (3) and the He–He potential V_{12}, Eq. (4), are expanded in Legendre polynomials using 100 Gauss–Legendre quadrature points. Finally, radial integrals are numerically evaluated.

IV. RESULTS

Due to the bosonic character of the ^{4}He atoms, all the calculations are performed imposing an even parity for their

TABLE I. Interaction energies (cm^{-1}) of the $^4He_2-N_2$ cluster at several distances of the diatomic bond r (Å). E^{QC}, from quantum chemistry calculations; $\langle L^2\rangle$, mean square orbital angular momentum (a.u.) from QC; $E^{QC}_{eff}(J)$, E^{QC} plus averaged rotational term; and $E^{AD}(J)$, from r-adiabatic calculations at a total angular momentum J; the inversion parity being $\varepsilon=(-1)^J$, and the N–N interchange $\eta=+1$.

r	E^{QC}	$\langle L^2\rangle$	$E^{QC}_{eff}(0)$	$E^{AD}(0)$	$E^{AD}(1)$	$E^{AD}(2)$
0.8996	−12.6330	2.5862	−4.9751	−11.0818	−10.0292	−9.5666
0.9525	−12.7997	2.3582	−6.5713	−11.4242	−10.3689	−9.9044
1.0054	−13.0050	2.1437	−7.9234	−11.7870	−10.7306	−10.2635
1.0583	−13.2275	1.9422	−9.0725	−12.1502	−11.0937	−10.6235
1.1112	−13.4027	1.7467	−10.0133	−12.4548	−11.4004	−10.9257
1.1642	−13.5884	1.5567	−10.8360	−12.7580	−11.7065	−11.2260
1.2171	−13.6967	1.3848	−11.4566	−12.9689	−11.9218	−11.4357
1.2700	−13.3996	1.2336	−11.5669	−12.7651	−11.7288	−11.2400
1.3229	−12.7889	1.1027	−11.2791	−12.2370	−11.2159	−10.7269
1.3758	−11.9885	0.9907	−10.7344	−11.5078	−10.5040	−10.0169
1.4287	−11.0833	0.8960	−10.0316	−10.6632	−9.6770	−9.1934
1.4816	−10.1306	0.8166	−9.2392	−9.7615	−8.7927	−8.3135
1.5346	−9.1684	0.7506	−8.4046	−8.8421	−7.8898	−7.4159
1.5875	−8.2217	0.6961	−7.5598	−7.9312	−6.9943	−6.5261
1.6404	−7.3063	0.6513	−6.7263	−7.0457	−6.1229	−5.6608
1.6933	−6.4317	0.6147	−5.9180	−6.1963	−5.2863	−4.8303
1.7462	−5.6033	0.5850	−5.1436	−5.3889	−4.4906	−4.0407
1.7992	−4.8233	0.5610	−4.4080	−4.6267	−3.7388	−3.2950
1.8521	−4.0922	0.5418	−3.7137	−3.9106	−3.0321	−2.5943

exchange, i.e., $\kappa=+1$. In QC calculations, the ground level obtained by solving Eq. (20) corresponds to a "Σ" state, i.e., $\Omega=0$.

The effect of decoupling the He-atom orbital angular momenta from the BC rotation is analyzed by comparing the results obtained from the QC and AD approaches. At several elongations of the N_2 bond, Table I collects the $E^{QC}(r)$ energies (column 2), the $\langle L^2\rangle$ values (column 3) providing the averaged diatomic rotation, Eq. (23), and the effective perturbation $E^{QC}_{eff}=E^{QC}(r)+\langle \mathbf{j}^2\rangle/2mr^2$ at $J=0$ (column 4). Also, in this table, we list the lowest AD energies obtained by solving Eq. (17) for $J=0$, 1, and 2 (columns 5–7). They correspond to states of symmetries $\eta=+1$ and $\varepsilon=(-1)^J$. As can be noticed, at $J=0$, the QC approach severely underestimates the binding energies with respect to the AD values at all the r distances, although this effect diminishes as r increases. It is a direct consequence of neglecting the coupling of the He orbital angular momenta and the diatomic rotation in the QC formulation, which is important for light dopants. Note that the binding energies reach their maximum values for r distances slightly stretched from the equilibrium ($r_e=2.0743a_0=1.0977$ Å). This is a dynamical effect associated with the already mentioned acuteness of the PES in the neighborhood of its global minimum, and is also seen through diabatic calculations as commented below.

The results of the precedent table are interpolated using cubic splines to obtain the corresponding perturbation to the diatomic potential energy within the QC and AD approaches. For each (J,v) state, we list in Table II the QC, AD, and D total energies of the system obtained by solving Eqs. (22) and (19), and the Schrödinger equation associated with the Hamiltonian of Eq. (16), respectively. For the sake of comparisons, the corresponding energies for the bare diatomic molecule are listed in the last column of this table. As already discussed,[20] for low vibrational excitations, the D values can be considered accurate as long as there is a large mismatch between the low frequency of the $He-N_2$ stretching and bending motions, and the high frequency of the N_2 vibration. As a rule, the accord between AD and D results is always better than 0.01 cm^{-1} showing the adequacy of a Born–Oppenheimer separation of the r coordinate from the rest. In turn, the difference between QC and AD values ranges, according to the results shown in Table I, from more than 2 cm^{-1} at $J=0$ to more than 12 cm^{-1} at $J=2$ whatever

TABLE II. Total energies (cm^{-1}) of the cluster for selected (J,v) states from QC, AD and D calculations [$\varepsilon=(-1)^J$, and $\eta=+1$, for AD and D approaches]. The corresponding energies for the bare $N_2(X)$ molecule are also listed in the last column.

(J,v)	QC	AD	D	$N_2(X)$
(0,0)	−78735.2424	−78737.8295	−78737.8351	−78725.4307
(1,0)	−78731.2650	−78736.7748	−78736.7801	−78721.4531
(2,0)	−78723.3103	−78736.3008	−78736.3064	−78713.4982
(0,1)	−76408.2035	−76410.7446	−76410.7549	−76398.3093
(1,1)	−76404.2627	−76409.6927	−76409.7003	−76394.3684
(2,1)	−76396.3813	−76409.2175	−76409.2259	−76386.7868

TABLE III. Energy difference (cm^{-1}) between the incoming and outgoing photons, for allowed Raman transitions $(J',v'=1)\leftarrow(J,v=0)$ in the infrared region from QC, AD, and D calculations. For QC and D, intensities in parenthesis (arbitrary units) are also included.

Branch	QC	AD	D
$O(2)$	$2315.1068(1.0\times10^{-18})$	2325.5542	$2325.5515(4.8\times10^{-8})$
$P(2)$	2319.0476(0)	2326.6081	$2326.6061(2.2\times10^{-9})$
$Q(0)$	$2327.0389(3.5\times10^{-2})$	2327.0829	$2327.0802(3.5\times10^{-2})$
$Q(1)$	$2327.0023(3.9\times10^{-7})$	2327.0821	$2327.0798(1.9\times10^{-3})$
$Q(2)$	$2326.9290(4.4\times10^{-17})$	2327.0833	$2327.0805(7.4\times10^{-5})$
$R(1)$	2334.8837(0)	2327.5573	$2327.5542(6.0\times10^{-9})$
$S(0)$	$2338.8611(4.1\times10^{-3})$	2338.5012	$2338.4954(3.7\times10^{-3})$

the vibrational state. Thus, as expected, neglecting Coriolis couplings leads to worse and worse QC results as J increases.

However, in spite of this discrepancy, the QC approach is able to reproduce the most intense branches of the vibrotational $(v=1\leftarrow0)$ Raman spectrum. We show in Table III the line positions obtained by means of the three approaches. The corresponding intensities obtained (at a temperature of 0.5 K) from QC (Refs. 14 and 15) and D, Eq. (29), treatments are also shown in this table. The necessary spherical and anisotropic parts of the N_2 polarizability are taken from Ref. 41. Within the QC approach, the position of the most intense branch $Q(0)$ deviates from AD and D exact values by $\sim5\times10^{-2}$ cm^{-1}, the corresponding intensity also being predicted with high accuracy. The following most intense branch, $S(0)$, is located with an error of ~0.3 cm^{-1}. Its intensity is overestimated only by $\sim10\%$. For the rest of allowed branches involving $J\neq0$ states, the QC intensities become meaningless. On the other hand, note that in contrast to the QC prediction, P and R branches are allowed in the exact treatment, although with almost negligible intensities.

An important issue in the field of doped clusters is the evolution of effective moments of inertia with the cluster size.[42,43] Assuming that the dopant molecule is only slightly perturbed by the environment, and neglecting centrifugal distortions, cluster energy levels can be approximated as[17] $E_{Jv}\approx E_{0v}+B_vJ(J+1)$, where E_{0v} are the corresponding rotationless $(J=0)$ energies, while B_v are effective rotational constants depending on the vibrational excitation. For the case under study involving just two He atoms, the difference of the positions between the more intense $S(0)$ and $Q(0)$ lines, Δ_{SQ} can be used to estimate an effective rotational constant at the $v=1$ excited level as $B_1=\Delta_{SQ}/6$. Thus, the QC and D approaches produce values (in cm^{-1}) of 1.970 367 and 1.902 533, respectively, i.e., the QC treatment overestimates B_1 by $\approx4\%$. Since the rotational constant of the isolated N_2 molecule at $v=1$ is 1.970 450 cm^{-1}, its apparent moment of inertia increases (as expected) in the presence of He atoms, although it remains almost unaltered when calculated by means of the QC approach.

Figure 2 displays the more intense Q and S branches of the simulated vibrotational Raman stick spectrum, at a temperature of 0.5 K, obtained through QC and D approaches. It clearly shows the degree of agreement attained by the two formulations. For the $S(0)$ branch the accord is remarkably good, and for $Q(0)$ is excellent. Note the presence of a $Q(1)$ branch within the exact treatment that is not reproduced by the QC formalism. Its intensity, however, is ~20 times lower than that of $Q(0)$.

The surprising "good" QC result for the $S(0)$ branch, which, in fact, involves an excited $J=2$ state, deserves a further explanation. Such result is a direct consequence of the selection rules mentioned above. First of all, at low temperatures, the Boltzmann distribution privileges the contribution of the lowest energy states as origin of each transition. Accordingly, in Table IV we show the $v=0$ and 1 diabatic states which have been found for $J=0$ and 2 of $\eta=\epsilon=(-1)^L=+1$ symmetry (note, again, that the cluster is bounded more at $v=1$ than at $v=0$). Those states are the main candidates to contribute to the $S(0)$ and $O(2)$ lines. Taking into account the criterion of temperature, the origin of $S(0)$ is presumably the ground state of $J=v=0$ placed at $\simeq12.40$ cm^{-1}. Due to the Ω conservation, the final state should be the sixth excited level of $J=2$, $v=1$ which amounts the largest component on $\Omega=0$. As can be realized in Table III, this is indeed the case (the energy associated with the vibrational $v'=1\leftarrow v=0$ excitation of the bare N_2 molecule at $J=0$ is ~2327.12 cm^{-1}). Such state is placed at $\simeq1.03$ cm^{-1}, meaning that, apart from the small variation

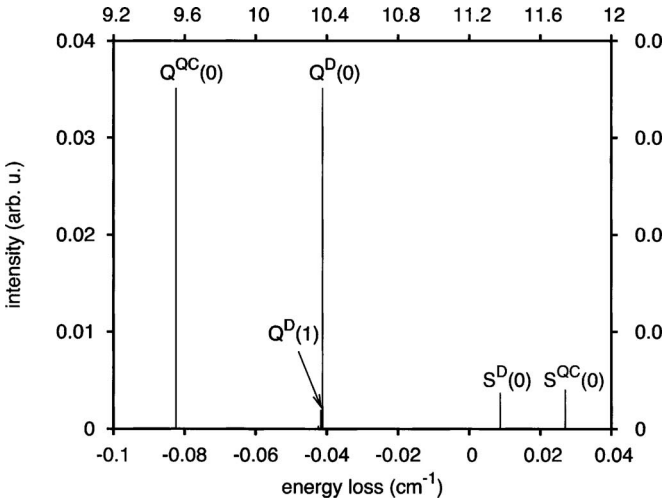

FIG. 2. Main branches of the $(v=1\leftarrow0)$ vibrotational Raman spectrum (Stokes region) in terms of the energy loss between the incident and the exiting photons, $\hbar\omega_0-\hbar\omega_{fi}$, measured with respect to the (forbidden) transition of the bare dopant $(J,v)=(0,1)\leftarrow(0,0)$, 2327.121 415 cm^{-1}. The bottom x axis is associated with Q branches, while the top x axis corresponds to S branches.

TABLE IV. Diabatic states at $J=0$ and 2 for quantum numbers $\eta=\varepsilon=(-1)^L=1$: Binding energies ($cm^{-1}$) and weights (%) of the Ω components.

J	$v=0$	$v=1$	$\Omega=0/1/2$
0	−12.404	−12.446	100/0/0
	−10.770	−10.813	
	−7.1760	−7.2220	
	−1.9119	−1.9621	
2	−10.876	−10.917	18/36/46
	−9.9984	−10.040	21/39/40
	−8.8262	−8.8689	21/40/39
	−6.4106	−6.4560	22/40/38
	−5.3342	−5.3800	21/39/40
	−1.2115	−1.2613	22/40/38
	−0.83038	−1.0300	93/1/6
	−0.13178	−0.18212	21/39/40

coming from the vibrational excitation and the presence of He atoms, the N_2 rotor is mainly executing a $j'=2\leftarrow j=0$ transition (the rotational constant of this molecule is $\sim 2\ cm^{-1}$). Thus, and considering the additional L conservation, this is a manifestation of the accuracy of the rotational term accounted for in the QC approach for the $S(0)$ branch. The case of $O(2)$ is completely different as the initial state corresponds to the ground level at $J=2$, $v=0$ while the final one is also the ground level at $J=0$, $v=1$. Hence, the transition, which is placed a couple of wavenumbers down to the N_2 vibrational excitation, cannot be reproduced within the QC approach. The small component of the initial state on $\Omega=0$ explains the very low intensity found for this transition.

V. SUMMARY AND OUTLOOK

The assumptions involved in a QC-like treatment of diatomic molecules embedded in helium clusters have been tested on the $^4He_2-N_2(X)$ system using a model PES which consists in the addition of *ab initio* triatomic $He-N_2$ potentials plus the He–He interaction. To this end, we perform a study of the energies of the system and present simulated vibrotational Raman spectra within QC as well as AD and D (exact) treatments. Our main conclusions are as follows.

(1) Adiabaticity of the diatomic stretch is accurate to within 0.01 wavenumbers with respect to the diabatic, exact treatment, and constitutes an acceptable approximation.

(2) Decoupling of BC rotation from the He angular momenta is the main source of discrepancies when one compares QC with AD or exact results, and its effect is magnified when light dopants are contained in the cluster. Thus, for this system, energy differences higher than 2 cm^{-1} are already found at $J=0$. Since Coriolis couplings are neglected those energy differences increase with J.

(3) However, at low temperatures, the QC treatment provides a good description of the main features associated with the vibrotational Raman spectroscopy of this cluster. This is due to the main contribution of initial $J=0$ states together with the selection rules. Thus, and since the diatomic dopant is only slightly perturbed by the environment of He atoms, the QC approach accurately describes the most intense $Q(0)$ and $S(0)$ lines of spectrum.

Up to date the QC model has been applied using Hartree (or Hartree–Fock, for fermions) approaches to study larger aggregates at the same level of accuracy.[14–19] Such treatments involve their own limitations, and therefore the use of higher level *ab initio* methodologies would be desirable. Work in this direction has already started with the implementation of a Jacobi–Davidson based full interaction configuration (FCI) treatment for studying small doped ^3He_N clusters,[44] its extension for dealing with boson and mixtures of boson/fermion environments being in progress. Since this methodology allows the calculation not only of the ground level but also of excited states, it could serve as a starting point to account for the coupling among rotational motions within a prediagonalization scheme.[20] In addition, in order to achieve an accurate description of ground and excited states of larger clusters, less expensive *ab initio* treatments than the FCI one, based on the analysis of the pair correlation function, are envisaged.

ACKNOWLEDGMENTS

This work has been partially supported by the DGICYT Spanish Grant Nos. FIS2007-62006 and CTQ2004-02415/BQU. M.P.deL.-C. acknowledges the support of a MEC-CSIC Spanish Grant No. 2007501004. The calculations presented here were performed at Centro de Cálculo of IMAFF (CSIC).

[1] S. Goyal, D. L. Schutt, and G. Scoles, Phys. Rev. Lett. **69**, 933 (1992).
[2] M. Hartmann, R. E. Miller, J. Toennies, and A. F. Vilesov, Phys. Rev. Lett. **75**, 1566 (1995).
[3] C. Callegari, K. K. Lehmann, R. Schmied, and G. Scoles, J. Chem. Phys. **115**, 10090 (2001).
[4] J. P. Toennies and A. F. Vilesov, Angew. Chem., Int. Ed. **43**, 2622 (2004).
[5] K. Nauta and R. E. Miller, J. Chem. Phys. **115**, 10138 (2001).
[6] K. Nauta and R. E. Miller, J. Chem. Phys. **117**, 4846 (2002).
[7] C. M. Lindsay and R. E. Miller, J. Chem. Phys. **122**, 104306 (2005).
[8] J. Tang and A. R. W. McKellar, J. Chem. Phys. **119**, 754 (2003).
[9] A. R. W. McKellar, J. Chem. Phys. **121**, 6868 (2004).
[10] S. Grebenev, J. P. Toennies, and A. F. Vilesov, Science **279**, 2083 (1998).
[11] S. Grebenev, M. Hartmann, M. Havenith, B. Sartakov, J. P. Toennies, and A. F. Vilesov, J. Chem. Phys. **112**, 4485 (2000).
[12] M. Barranco, R. Guardiola, S. Hernández, R. Mayol, J. Navarro, and M. Pí, J. Low Temp. Phys. **142**, 1 (2006).
[13] P. Jungwirth and A. I. Krylov, J. Chem. Phys. **115**, 10214 (2001).
[14] D. López-Durán, M. P. de Lara-Castells, G. Delgado-Barrio, P. Villarreal, C. Di Paola, F. A. Gianturco, and J. Jellinek, Phys. Rev. Lett. **93**, 053401 (2004).
[15] D. López-Durán, M. P. de Lara-Castells, G. Delgado-Barrio, P. Villarreal, C. Di Paola, F. A. Gianturco, and J. Jellinek, J. Chem. Phys. **121**, 2975 (2004).
[16] M. P. de Lara-Castells, D. López-Durán, G. Delgado-Barrio, P. Villarreal, C. Di Paola, F. A. Gianturco, and J. Jellinek, Phys. Rev. A **71**, 033203 (2005).
[17] M. P. de Lara-Castells, R. Prosmiti, G. Delgado-Barrio, D. López-Durán, P. Villarreal, F. A. Gianturco, and J. Jellinek, Phys. Rev. A **74**, 053201 (2006).
[18] P. Villarreal, M. P. de Lara-Castells, R. Prosmiti, G. Delgado-Barrio, D. López-Durán, F. A. Gianturco, and J. Jellinek, Phys. Scr. **76**, C96 (2007).
[19] M. P. de Lara-Castells, R. Prosmiti, D. López-Durán, G. Delgado-Barrio, P. Villarreal, F. A. Gianturco, and J. Jellinek, Int. J. Quantum Chem. **107**,

2902 (2007).
[20] O. Roncero, R. Pérez-de Tudela, M. P. de Lara-Castells, R. Prosmiti, G. Delgado-Barrio, and P. Villarreal, Int. J. Quantum Chem. **107**, 2756 (2007).
[21] P. Villarreal, O. Roncero, and G. Delgado-Barrio, J. Chem. Phys. **101**, 2217 (1994).
[22] M. I. Hernández and N. Halberstadt, J. Chem. Phys. **100**, 7828 (1994).
[23] M. I. Hernández, N. Halberstadt, W. D. Sands, and K. C. Janda, J. Chem. Phys. **113**, 7252 (2000).
[24] A. Heidenreich, U. Even, and J. Jortner, J. Chem. Phys. **115**, 10175 (2001).
[25] A. Heidenreich and J. Jortner, J. Chem. Phys. **118**, 10101 (2003).
[26] P. M. Felker and D. Neuhauser, J. Chem. Phys. **119**, 5558 (2003).
[27] A. Valdés, R. Prosmiti, P. Villarreal, and G. Delgado-Barrio, J. Chem. Phys. **122**, 044305 (2005).
[28] P. M. Felker, J. Chem. Phys. **125**, 184313 (2006).
[29] J. A. Beswick and J. Jortner, Adv. Chem. Phys. **47**, 363 (1981).
[30] E. B. Wilson, Jr., J. C. Decius, and P. C. Cross, *Molecular Vibrations: The Theory of Infrared and Raman Vibrational Spectra* (McGraw-Hill, New York/Dover, New York, 1955).
[31] R. Prosmiti, C. Cunha, P. Villarreal, and G. Delgado-Barrio, J. Chem. Phys. **116**, 9249 (2002).
[32] A. Valdés, R. Prosmiti, P. Villarreal, and G. Delgado-Barrio, Mol. Phys. **102**, 2277 (2004).
[33] R. Prosmiti, C. Cunha, P. Villarreal, and G. Delgado-Barrio, J. Chem. Phys. **117**, 7017 (2002).
[34] A. Valdés, R. Prosmiti, P. Villarreal, and G. Delgado-Barrio, J. Chem. Phys. **125**, 014313 (2006).
[35] T. Stoecklin, A. Voronin, A. K. Dham, J. S.-F. Stoker, and R. W. McCourt, Mol. Phys. **106**, 75 (2008).
[36] T. Stoecklin, A. Voronin, and J. C. Rayez, Phys. Rev. A **66**, 042703 (2002).
[37] T. S. Ho and H. Rabitz, J. Chem. Phys. **104**, 2584 (1996).
[38] A. J. C. Varandas and J. D. Silva, J. Chem. Soc., Faraday Trans. **88**, 941 (1992).
[39] Z. Bačić, M. Kennedy-Mandzink, J. W. Moskowitz, and K. E. Schmidt, J. Chem. Phys. **97**, 6472 (1992).
[40] R. A. Aziz and M. J. Slaman, J. Chem. Phys. **94**, 8047 (1991).
[41] G. Maroulis, J. Chem. Phys. **118**, 2673 (2003).
[42] Y. Xu, N. Blinov, W. Jager, and P.-N. Roy, J. Chem. Phys. **124**, 081101 (2006).
[43] W. Topic, W. Jager, N. Blinov, P.-N. Roy, M. Botti, and S. Moroni, J. Chem. Phys. **125**, 144310 (2006).
[44] M. P. de Lara-Castells, G. Delgado-Barrio, P. Villarreal, and A. O. Mitrushchenkov, J. Chem. Phys. **125**, 221101 (2006).